NASA TECHNICAL MEMORANDUM

NASA TM X-52941

PERFORMANCE OF NOISE SUPPRESSORS FOR A FULL-SCALE FAN FOR TURBOFAN ENGINES

by Edward J. Rice
Lewis Research Center
Cleveland, Ohio

TECHNICAL PAPER proposed for presentation at
Ninth Aerospace Sciences Meeting sponsored by the
American Institute of Aeronautics and Astronautics
New York, New York, January 25-27, 1971

PERFORMANCE OF NOISE SUPPRESSORS FOR A FULL-SCALE FAN FOR TURBOFAN ENGINES

by Edward J. Rice
National Aeronautics and Space Administration
Lewis Research Center
Cleveland, Ohio

Abstract

Inlet and exhaust noise suppressors for a 6 foot (1.83 m) diameter fan for a high by-pass ratio turbofan engine were tested. The perforated plate on honeycomb suppressors provided a much broader band noise attenuation than was predicted. Perceived noise level attenuations due to the suppressors of 13 and 12 PNdB were obtained for simulated approach and take-off conditions respectively.

The theory used for the design of the suppressors is discussed. In general, the theory predicts the frequency for peak attenuation but underpredicts the peak attenuation amplitude. For frequencies above and below peak, the observed attenuations are more than predicted.

Degradations of the aerodynamic performance due to the noise suppressors were smaller than the experimental errors which were estimated to be 2%.

E-5878

Symbols

B_j	coefficient for the j^{th} characteristic function of acoustic pressure
b	backing depth of liner resonators, ft
c	speed of sound, ft/sec
d	perforated plate hole diameter, ft
E	acoustic power, ft-lb_f/sec
E_{jk}	acoustic power contribution of the j^{th} and k^{th} pressure or velocity solutions, ft-lb_f/sec
ΔdB	sound power attenuation
f	sound frequency, Hz
H	duct height, ft
I	axial acoustic power flux, lb_f/sec/ft
I_{jk}	acoustic power flux contribution of the j^{th} and k^{th} pressure or velocity solutions, lb_f/sec/ft
i	$\sqrt{-1}$
L	length of acoustic treatment, ft
ℓ	perforated plate sheet thickness, ft
M	average steady flow Mach number
p	acoustic pressure, lb_f/ft^2
p_j	acoustic pressure contribution of j^{th} characteristic function, lb_f/ft^2
p_j^*	complex conjugate of p_j, lb_f/ft^2
Q_j	$1 - M(\tau_j - i\sigma_j)$
S/A	ratio of acoustic treatment area to duct cross-sectional area
t	time, sec
v_j	acoustic particle velocity contribution of j^{th} characteristic function, ft/sec
v_n	normal acoustic particle velocity at a lined wall, ft/sec
v_o	orifice gas velocity in Helmholtz resonator, ft/sec
v_x	axial component of acoustic particle velocity Σv_{xj}, ft/sec
v_{xj}	axial component of v_j, ft/sec
v_y	transverse component of acoustic particle velocity Σv_{yj}, ft/sec
v_{yj}	transverse component of v_j, ft/sec
x	axial coordinate, ft
y	transverse coordinate, ft
Z	liner acoustic impedance, lb_m/ft^2/sec
α_j	complex eigenvalue of j^{th} transverse characteristic solution
δ	orifice end correction
η	frequency parameter (Hf/c)
θ	specific acoustic resistance
θ_{NL}	nonlinear specific acoustic resistance
ν	gas kinematic viscosity, ft^2/sec
ρ	density, lb_m/ft^3
σ	open area ratio (orifice area to wall area)
σ_j, τ_j	transmission parameters for j^{th} characteristic function (see eq. (6))

χ specific acoustic reactance

ω angular frequency

$( )^*$ complex conjugate

Introduction

Current four engine aircraft using ducted fans of the 707/DC-8 class produce about 120 PNdB of noise at standard measuring points during both takeoff and landing. The NASA Quiet Engine Program was initiated to demonstrate the feasibility of reducing this noise by 15 to 20 PNdB by engine design changes and perhaps another 10 PNdB by the use of absorptive duct liners. In support of these goals, a facility described in Ref. 1, has been built for determing the performance and noise characteristics of full-scale fans. Performance and noise data without acoustic treatment are reported in Ref. 2 for the first 6 foot (1.83 m) diameter fan tested, and the complete acoustic data with acoustic liners are presented in Ref. 3.

This paper describes the noise reduction attained by the use of acoustic liners in the inlet and exhaust ducts of the fan. The use of acoustic treatment to suppress engine noise has recently received considerable attention. Numerous experimental and analytical studies have been performed to develop liner design methods[4, 5].

The liners used in this study were of a perforated plate-honeycomb construction. They were designed using the results of a sound transmission model. A comparison of experimental and theoretical results is presented. Estimates of the flyover noise characteristics (without core engine noise) of an airplane having this fan and treatment on four engines are given.

Analytical Model

The geometry upon which the present theory is based is shown in Fig. 1. The model is the same as in Ref. 6 except that rectangular instead of cylindrical geometry is used.

The sound-pressure waves will enter the duct at $x = 0$ and run in the positive x-direction. A positive Mach number will indicate steady flow in the positive x-direction thus simulating a fan exhaust condition. A negative Mach number simulates a fan inlet.

Additional assumptions made in the analysis are as follows. The sound-pressure level in the duct is sufficiently small that the linearized wave equation may be used. The steady flow in the duct is uniform. The duct is properly terminated or of sufficient length such that no end reflections occur. The wall impedance is uniform and does not change with length. This last assumption can be relaxed by matching the solutions at the joining planes of several short ducts within which the wall impedance can be considered not to vary.

The linearized wave equation with uniform steady flow is

$$\nabla^2 p = \frac{1}{c^2}\frac{\partial^2 p}{\partial t^2} + \frac{2M}{c}\frac{\partial^2 p}{\partial x\,\partial t} + M^2\frac{\partial^2 p}{\partial x^2} \tag{1}$$

With the left side of Eq. (1) expressed in rectangular coordinates, the symmetric, separable solutions for acoustic pressure that are periodic in time can be written as

$$p_j = B_j e^{i\omega t}\cos(2\alpha_j y/H)e^{-(\omega/c)(\sigma_j + i\tau_j)x} \tag{2}$$

The j subscript indicates an infinite number of characteristic solutions are available. The complete solution for pressure is then

$$p = \sum_j p_j \tag{3}$$

The acoustic particle velocity that is periodic in time and exponential in x corresponding to each of the characteristic solutions in pressure is

$$v_j = (i/\rho\omega Q_j)\nabla p_j \tag{4}$$

where

$$Q_j = 1 - M(\tau_j - i\sigma_j) \tag{5}$$

and again the velocity is built up by the summation of the infinite number of characteristic solutions.

The damping and transmission parameters in Eq. (2) are related to the Mach number and transverse eigenvalues by

$$\sigma_j + i\tau_j = \left[-iM + \sqrt{(1 - M^2)(\alpha_j/\pi\eta)^2 - 1}\right]\Big/(1 - M^2) \tag{6}$$

where

$$\eta = Hf/c \tag{7}$$

The eigenvalues α_j and pressure coefficients B_j in Eq. (2) must be evaluated by the use of boundary conditions imposed at the acoustic liner surface and the duct entrance. Both α_j and B_j may be complex numbers.

Boundary Conditions

At the acoustic liner surfaces ($y = \pm H/2$), each characteristic solution must be compatible with the wall-impedance condition. The wall impedance must be specified by some independent method. The wall impedance is defined as the ratio of acoustic pressure to acoustic velocity normal to the wall. Thus the acoustic impedance is given by

$$Z = (p_j/v_{yj})_{y=H/2} \qquad j = 1, 2, 3, \ldots \tag{8}$$

When Eqs. (2) and (4) are used in Eq. (8), the boundary condition can be expressed as

$$Z/\rho c\eta = \left[i\pi\cos(\alpha_j)/\alpha_j\sin(\alpha_j)\right]Q_j \tag{9}$$

Equation (9) can then be solved for each of the α_j. Q_j also contains α_j through σ_j and τ_j, which renders the

system nonorthogonal. For $M = 0$, Q_j equals 1 and the solutions are orthogonal.

It should be noted that the wall-boundary condition as expressed in Eq. (9) uses the particle-velocity continuity concept rather than the continuity of particle-displacement concept. If continuity of particle displacement is used at the liner wall, Q_j will appear in Eq. (9) to the second power.

The second boundary condition involves specifying the pressure wave at the lined duct entrance ($x = 0$). It is assumed here that this pressure wave is plane and periodic. This condition can be written as

$$p = \sum_j p_j = e^{i\omega t} \qquad (x = 0) \tag{10}$$

Using Eq. (2) in Eq. (10) yields

$$\sum_j B_j \cos(2\alpha_j y/H) = 1 \tag{11}$$

Multiplying by $\cos(2\alpha_k y/H)$ and integrating from $y = -(H/2)$ to $+(H/2)$ transforms Eq. (11) into

$$\sum_j B_j \int_{-(H/2)}^{+(H/2)} \cos(2\alpha_j y/H)\cos(2\alpha_k y/H)dy = \int_{-(H/2)}^{+(H/2)} \cos(2\alpha_k y/H)dy \tag{12}$$

If the system of solutions were orthogonal (as when $M = 0$), the integral on the left of Eq. (12) would equal zero except for $k = j$. A single equation would then result for each of the B_j. However, for nonzero Mach number all of the integrals in Eq. (12) may be nonzero. The result is an infinite number of linear equations each containing all of the B_j's. The system of equations can be truncated at the number of terms that provides sufficient accuracy. For the results presented in this paper, the first 10 characteristic functions were used.

Sound-Power Attenuation

The sound-power flux in the axial direction for the present case of uniform steady flow can be written as

$$I = pv_x + M/2\left[(p^2/\rho c) + \rho c\left(v_x^2 + v_y^2\right)\right] \tag{13}$$

This can be obtained by substitution of the first-order continuity and momentum equations into the energy equation carried to the second order, with only time-varying terms considered.

Because the pressures and velocities in Eq. (13) are summations of complex quantities, the jk^{th} term of the sound power flux can be written:

$$I_{jk} = (1/2)\text{Real}\left\{p_j^* v_{xk} + (M/2)\left[(p_j^* p_k/\rho c) + \rho c(v_{xj}^* v_{xk} + v_{yj}^* v_{yk})\right]\right\} \tag{14}$$

where p_j^* is the complex conjugate of the j^{th} term in the pressure series.

The jk^{th} term in the sound power series is then

$$E_{jk} = \int_{-(H/2)}^{+(H/2)} I_{jk}\, dy \tag{15}$$

The sound power E is then obtained by summing Eq. (15) over j and k.

The sound power can then be calculated at $x = 0$ and $x = L$ and the sound power attenuation then is given by

$$\Delta \text{ dB} = 10 \log_{10}\left[(E_{x=L})/(E_{x=0})\right] \tag{16}$$

Wall Impedance Model

Equation (9) contains the acoustic impedance of the wall. The following equations relate the acoustic impedance to the geometric variables of a perforated plate wall and to the acoustic and flow environment. The equations, or in some cases the data from which the equations were determined, are available in the literature and are reviewed in Ref. 7.

The specific acoustic impedance is defined as:

$$(p/\rho c v_n) = \theta + i\chi \tag{17}$$

the resistance is given by:

$$\theta = \left(\sqrt{8\nu\omega/\sigma c}\right)\left[1 + (\ell/d)\right] + \theta_{NL} \tag{18}$$

where

$$\theta_{NL} = \left(|v_o|/\sigma c\right)(1 + 6.67\,|M|) \tag{19}$$

The first term in Eq. (18) is the linear resistance of a Helmholtz resonator array due to viscous dissipation in the oscillatory boundary layers at the walls and in the orifice. In the absence of steady grazing flow and for very small sound levels, this is the entire acoustic resistance of the wall.

The second term in Eq. (19) was empirically derived to account for the increase in acoustic resistance of the wall due to grazing flow. The peak orifice velocity accounts for the nonlinear acoustic resistance due to finite pressure amplitude, and is related to the pressure amplitude by:

$$|v_o| = (|p|)\Big/\left(\rho c\sigma\sqrt{\theta^2 + \chi^2}\right) \tag{20}$$

The specific acoustic reactance of the wall can be expressed as:

$$\chi = \left[\omega(\ell + \delta)/\sigma c\right] - \cot(\omega b/c) \tag{21}$$

where δ is the orifice end correction and is given by:

$$\delta = 0.85\, d\left(1 - 0.7\sqrt{\sigma}\right)\Big/(1 + 305\, M^3) \tag{22}$$

When the liner geometry, flow conditions, and noise spectrum are given, Eqs. (18) to (20) must be solved by

iteration for θ. The reactance is obtained directly from Eqs. (21) and (22).

Equations (18) to (22) were used to define the impedance which was used to calculate the theoretical noise attenuations presented in Figs. 6 to 9. The noise spectra were characterized by their overall sound pressure levels. This peak pressure was used in Eq. (20) to define the peak orifice velocity. This approach was used with some success in Ref. 7 to correlate the results of a two-frequency resistance experiment.

Another approach could also be used. The peak pressure for each 1/3 octave center frequency could be inserted in Eq. (20) to obtain a peak orifice velocity. A resultant peak velocity could then be calculated by taking the square root of the sum of the squares of the individual velocities. This resultant velocity is then used in Eq. (19). An iteration procedure is required to determine the resistance. With this method the wall resistance is essentially constant with frequency. Only the linear resistance term (first term in Eq. (18)) which is usually small) varies with frequency. However, when the overall sound pressure level is used to characterize the noise spectrum (the method of the previous paragraph), the resistance is a stronger function of frequency.

Apparatus

Fan Description

A cutaway view of the fan can be seen in Fig. 2. The single stage fan has a large rotor-stator spacing (3.6 rotor chords) and is without inlet guide vanes. The fan is driven by electric motors through the shaft shown emerging from the fan inlet.

The detailed design of the fan in given in Ref. 1. The following fan parameters are given here for convenience. Aerodynamic parameters are corrected to standard sea level atmosphere of 518.7° R (288.2° K) and 2116.2 psf (1.013×10^5 N/m^2).

Rotor tip diameter, in. (m)	71.81 (1.8240)
Stator tip diameter, in. (m)	67.94 (1.7257)
Rotor tip speed (cruise design corrected value) at 3533 rpm, ft/sec (m/sec)	1107 (337.4)
Design stagnation pressure ratio	1.5
Design weight flow (corrected value), lbm/sec (kg/sec)	873 (396)
Rotor hub-tip ratio (inflow face)	0.50
Stator hub-tip ratio	0.59
Rotor to stator spacing (trailing to leading edges), in. (cm)	20 (50.8)
Rotor blading 53 blades (chord), in. (cm)	5.5 (13.97)
Stator blading 112 blades (chord), in. (cm)	2.69 (6.83)

Noise Suppressor Construction

The inlet and exhaust noise suppressors can be seen in Fig. 2. The inlet suppressor consists of a lined outer cowl and three splitter rings with acoustic lining on both sides. The exhaust suppressor has only the lined outer cowl and centerbody.

The suppressor dimensions and materials used in the acoustic liners are shown in Fig. 3. The liner is constructed with a perforated aluminum sheet bonded to a honeycomb backing. All facing materials are 0.020 inch (0.51 mm) thick perforated aluminum sheet metal. The three surface treatments indicated on the inlet differ only in the thickness of the honeycomb backing material.

Acoustic Power Comparisons - Hard and Soft Ducts

Several acoustic power spectra are presented in Figs. 4 and 5. The inlet and exhaust powers are determined by summation of the power in the front and rear hemispheres. The 90- and 60-percent speeds are representative of take-off and landing engine speeds. On each figure data for long and short inlets are shown with and without acoustic treatment.

The short inlet has the dimensions shown in Fig. 3. The long inlet is a result of adding a 41-inch (1.04-m) extension to the short inlet. It is clear from Figs. 4 and 5 that noise floors have been reached with the short inlet except at the blade passage frequency in Fig. 4. The noise floor in Fig. 5 is apparently a jet noise floor. The data with noise suppression is characteristic of jet noise up to a frequency of about 2000 Hz. The low frequency noise has a peak at about 125 Hz and then steadily falls off up to 2000 Hz, above which the internal noise dominates.

The suppressors are seen to provide large sound power attenuations over a very wide frequency range, especially for the forward radiated noise shown in Fig. 4. The noise attenuations will be considered in more detail in the next secion.

Acoustic Power Attenuations - Experimental and Theoretical

The experimental acoustic power attenuations for the exhaust and short inlet suppressors at 60- and 90-percent speed are shown in Figs. 6 to 9. These attenuations are the differences between the hard and soft cowl (short inlet) curves such as were shown in Figs. 4 and 5.

Theoretical predictions of suppressor performance are also shown in Figs. 6 to 9. The attenuation theory was based upon the model presented earlier in this paper. The rectangular geometry is intended to approximate the annular geometry of the suppressors. The model assumes a plane pressure wave enters the duct traveling in the direction of the duct axis. A uniform steady flow field was assumed without boundary layers or velocity gradients over the duct. The wall impedance was calculated according to Eqs. (18) to (22). Estimates of the overall sound pressure level within the ducts were obtained from the hard cowl far field data. This pressure was used in Eq. (20) to define the nonlinear resistance.

The calculation method provides attenuations for semi-infinite rectangular ducts with the same impedance on both walls. For the inlet suppressor each passage has different materials and thus different impedances on opposing walls. To handle this situation a result from the approximate theory of Morse[8] was used. The sound power attenuation in a duct is approximated by

$$\Delta \text{ dB} \approx \left[-4.34\theta(S/A)/(\theta^2 + \chi^2)\right] \qquad (23)$$

where (S/A) is the ratio of treated surface area to duct cross-sectional area. When put in terms of (S/A), Eq. (23) provides an approximation for either circular or rectangular ducts. For the case of walls of different impedance on two sides of a duct the following procedure was used. The attenuation calculations were performed as if just one of the materials was present on both walls of the duct. The calculations were repeated with the second material. According to Eq. (23) the attenuation is approximately proportional to the area of acoustic treatment. The attenuation for each material was thus weighted by its proportion of the total area of acoustic treatment. The total attenuation was then the sum of these weighted attenuations.

When several lined passages are involved such as in the fan inlet suppressor, a uniform sound power flux was assumed at the duct inlets. In cases where a radial sound intensity profile is known to exist, this assumption should be changed.

Figures 6, 7, and 8 have several characteristics in common. For frequencies both high and low, in comparison to the frequency of maximum attenuation, the experimental sound power attenuation is considerably higher than that predicted by theory. This difference is probably greater than is indicated; it was pointed out in the previous section that noise floors may have been reached except at the blade passage frequency. Shorter liners may have yielded essentially the same experimental results, but then the associated theoretical curves would have been reduced.

Another common characteristic of the three figures is that the frequency for maximum sound power attenuation has been fairly well predicted. At approach speed (60%) the magnitude is also fairly well predicted.

The differences between theory and experiment at high and low frequencies are not easy to explain. For the low frequencies a different dependence of wall impedance on frequency than that of Eqs. (18) to (22) may provide better agreement between theory and experiment. However, for the high frequencies the sound power attenuations are near the theoretical maxima over a considerable frequency range. No real wall material could have the impedance characteristics which are necessary for this behavior[7]. This would require a resistance which increases and a reactance which becomes more negative (stiffness controlled) with increasing frequency.

A possible explanation, especially for the high frequencies, for the behavior of the experimental data is as follows. The present theory assumes an axially propagating sound wave (at the lined duct entrance) with no transverse wave motion. This is the most conservative estimate available. Most of the acoustic power is directed axially while only transversely directed power can be absorbed at the lined wall. The turning of the axial power into the walls must be accomplished by the proper impedance match between the duct and the wall. However, if some other mechanism exists which can redirect the acoustic power into the walls the attenuation might be greatly increased. Such a mechanism exists in the form of gradients in the steady flow velocity. Propagation of sound in a duct with sheared flow has been investigated in Refs. 9 to 12. When the ratio of sound wavelength to boundary layer thickness is less than or nearly equal to one, the acoustic energy can be drastically redistributed. The presence of the boundary layers alone in the exit duct may not be sufficient to account for the large high frequency attenuation. Some radial velocity gradients over the exit duct were observed downstream from the stators. Application of the theory of Ref. 12 with these velocity gradients may be sufficient to account for the larger attenuations.

For the inlet duct, refraction of sound in the boundary layers in the lined passages will direct the acoustic energy toward the center of the passage and, therefore, reduce attenuation. However, the sound waves may be refracted in velocity gradients across the duct in the axial space between the rotor blades and the trailing edges of the inlet splitter rings. The sound waves will then enter the lined splitter ring sections at an angle rather than purely axially. This will result in increased higher order transverse mode content with resulting increased acoustic power attenuation.

Some evidence to illustrate the above point is shown in Fig. 10. The calculated potential flow velocities are shown as a function of radial position and axial distance in front of the rotor. The velocity magnitude is shown, but the axial velocity constitutes the bulk of this velocity. Very large velocity gradients in the radial direction are seen near the outer portion of the duct. These gradients may be sufficient to refract the noise toward the duct centerline.

The comparison of theory and experiment in Fig. 9 yields the same results as the previous three figures only at high frequencies. At low frequencies there is virtually no experimental sound power attenuation. At intermediate frequencies (centered around 1600 Hz) the theory greatly over-predicts the attenuation. Both of these effects are probably caused by the emergence of the fan jet noise as the dominant source at low and intermediate frequencies. The rear end power spectra for the treated ducts in Fig. 5 support this contention. The jet noise is seen to peak at about 125 Hz and then steadily decrease up to 2000 Hz beyond which another noise source dominates. Once the suppressor has reduced the internal intermediate frequency noise to the level of jet noise which is produced externally, further reduction will not produce observable differences. At low frequencies where external jet noise already dominates over internally generated noise, the suppressor can produce no observable effect in the far field.

Perceived Noise Levels

The perceived noise levels for simulated take-off and approach conditions were calculated according to Ref. 13. For take-off the 90-percent speed acoustic data were corrected to 1000 ft (305 m) sideline data. For approach the 60-pereent speed data were used on a 375 ft (114 m) sideline. Four fans were considered.

At take-off the suppressors reduced the perceived noise level by 12 PNdB (105 to 93 PNdB) and at approach by 13 PNdB (106 to 93 PNdB). The current DC-8 figures given by Pendley and Marsh[14] are 117 PNdB at take-off (1000 ft, 304.8 m) and 120 PNdB at approach (370 ft, 112.8 m). The reductions in perceived noise level (using the acoustically treated fans) are thus 24 PNdB at take-off and 27 PNdB at approach. These noise reductions are obtained by considering the fan noise only, and will be realized only if the core jet and turbine noise can be kept below the fan noise in an actual engine.

Estimates of the effective perceived noise levels have been calculated for an aircraft with four turbofan engines. Again it is emphasized that these noise levels are valid only if the core engine noise is less than that of the suppressed fan noise. Both tone and time duration corrections are considered by use of the calculation procedure of Ref. 15. The effective perceived noise level calculations are made using the noise spectra from the standard nozzle, short inlet configurations. The following comparisons are made between the hard cowl and acoustically treated versions. For simulated take-off conditions the effective perceived noise level was reduced by 17 EPNdB (102.7 to 85.7 EPNdB) and for approach by 14.3 EPNdB (102.5 to 88.2 EPNdB). The effective perceived noise level calculations were made using a relative humidity of 70 percent and a temperature of 77° F (298.2° K). For take-off the climb-out angle was 5.6 degrees, the velocity along the flight path was 292 ft/sec (89 m/sec), and the engine centerline was 9.1 degrees from horizontal. For approach the glide angle was -3 degrees, the velocity along the flight path was 241 ft/sec (73.5 m/sec), and the engine centerline was 0.5 degree from horizontal.

Aerodynamic Performance with Acoustic Treatment

The internal flow losses of the nacelle cowling were not measured directly; but the installed fan performance was obtained with both hard and acoustic surfaces lining the cowling. These data are presented in the table for 60 and 90 percent fan speeds, which represent the landing and take-off operating conditions. Fan pressure ratios shown include the inlet cowling losses because the pressure rise was measured from ambient to the fan stator discharge. Thrust includes all the cowl losses because it is the momentum measured at the nacelle exhaust.

The data indicate that the acoustic liner did not degrade the fan performance as much as the long inlet cowling.

It should be noted that the differences shown are all within the experimental measurement error, which was estimated to be about 2 percent of the full speed values. These errors are 16 pounds per second (7.3 kg/sec) on air-flow, 0.01 on pressure ratio and 400 pounds force (1780 N) on thrust.

Summary of Results

The inlet and exhaust noise suppressors for a 6 foot (1.83 m) diameter fan have been tested. Some of the more important results were as follows:

1. The suppressors provided more peak noise attenuation and much broader band attenuation than was predicted.
2. The duct sound transmission theory predicted the frequency of peak attenuation fairly well. The exception occurred when a fairly obvious jet noise floor dominated at the frequency of predicted peak attenuation.
3. Some noise floors of unknown origin were apparently reached even with the short treated inlet.
4. The noise suppressors provided a noise reduction of 13 PNdB at simulated approach conditions and 12 PNdB at take-off compared to the fan noise produced with hard passages.
5. The suppressor and fan combination achieved significant noise reductions when compared to the current DC-8 aircraft. The simulated approach and take-off noise reductions were 27 and 24 PNdB, respectively. These results are obtained under the assumption that the core engine noise is insignificant.
6. The changes in the aerodynamic performance due to the noise suppressors were within the experimental error in their measurement.

References

1. Leonard, B. R., Schmiedlin, R. F., and Stakolich, E. G., "Acoustic and Aerodynamic Performance of a Six Foot Diameter Fan for Turbofan Engines. Part I Design of Facility and QF-1 Fan," NASA TN D-5877.

2. Goldstein, A. W., Lucas, J. G., and Balombin, J. R., "Acoustic and Aerodynamic Performance of a Six Foot Diameter Fan for Turbofan Engines. Part II Performance of QF-1 Fan in Nacelle without Acoustic Suppression," NASA TN D-6080.

3. Rice, E. J., Feiler, C. E., and Acker, L. W., "Acoustic and Aerodynamic Performance of a Six Foot Diameter Fan for Turbofan Engines. Part III Performance with Noise Suppressors," Proposed NASA Technical Note.

4. "Progress of NASA Research Relating to Noise Alleviation of Large Subsonic Jet Aircraft," SP-189, 1968, NASA, Washington, D.C.

5. "NASA Acoustically Treated Nacelle Program," SP-220, 1969, NASA, Washington, D.C.

6. Rice, E. J., "Propagation of Waves in an Acoustically Lined Duct with a Mean Flow," Basic Aerodynamic Noise Research, SP-207, 1969, NASA, Washington, D.C., pp. 345-355.

7. Groeneweg, J. F., "Current Understanding of Helmholtz Resonator Arrays as Duct Boundary Conditions," Basic Aerodynamic Noise Research, SP-207, 1969, NASA, Washington, D.C., pp. 357-368.

8. Morse, P. M., Vibration and Sound, 2nd ed., McGraw-Hill, New York, N.Y., 1948.

9. Pridmore-Brown, D. C., "Sound Propagation in a Fluid Flowing Through an Attenuating Duct," Journal of Fluid Mechanics, Vol. 4, Pt. 4, Aug. 1958, pp. 393-406.

10. Tack, D. H. and Lambert, R. F., "Influence of Shear Flow on Sound Attenuation in a Lined Duct," Journal of the Acoustical Society of America, Vol. 38, No. 4, Oct. 1965, pp. 655-666.

11. Mungur, P. and Gladwell, G. M. L., "Acoustic Wave Propagation in a Sheared Fluid Contained in a Duct," Journal of Sound and Vibration, Vol. 9, No. 1, Jan. 1969, pp. 28-48.

12. Mungur, P. and Plumblee, H. E., "Propagation and Attenuation of Sound in a Soft-Walled Annular Duct Containing a Sheared Flow," Basic Aerodynamic Noise Research, SP-207, 1969, NASA, Washington, D.C., pp. 305-327.

13. Anon., "Definitions and Procedures for Computing the Perceived Noise Level of Aircraft Noise," ARP 865A, Aug. 1969, SAE, New York, N.Y.

14. Pendley, R. E. and Marsh, A. H., "Noise Predictions and Economic Effects of Nacelle Modifications to McDonnell Douglas DC-8 Airplanes," Progress of NASA Research Relating to Noise Alleviation of Large Subsonic Jet Aircraft, SP-189, 1968, Washington, D.C., pp. 173-195.

15. Federal Aviation Regulations, Vol. III, Pt. 36 - Noise Standards: Aircraft Type Certification.

Speed,	Inlet	Wall material	Airflow		Pressure ratio	Thrust	
			lbm/sec	kg/sec		lb	N
60	Short	Hard	505	229	1.14	7 200	32 000
	Short	Lined	493	224	1.14	7 400	32 900
	Long	Hard	484	220	1.15	7 200	32 000
	Long	Lined	486	220	1.14	7 200	32 000
90	Short	Hard	741	336	1.36	16 700	74 300
	Short	Lined	749	340	1.36	16 800	74 700
	Long	Hard	736	334	1.36	16 400	73 000
	Long	Lined	739	335	1.35	16 400	73 000

TABLE I. - AERODYNAMIC PERFORMANCE COMPARISONS

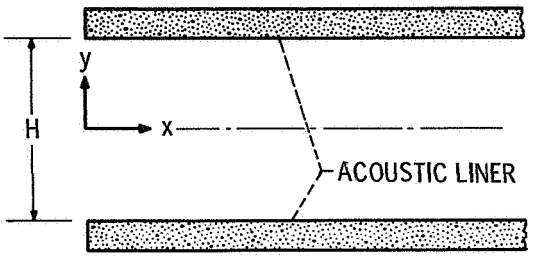

Figure 1. - Geometry for analytical model.

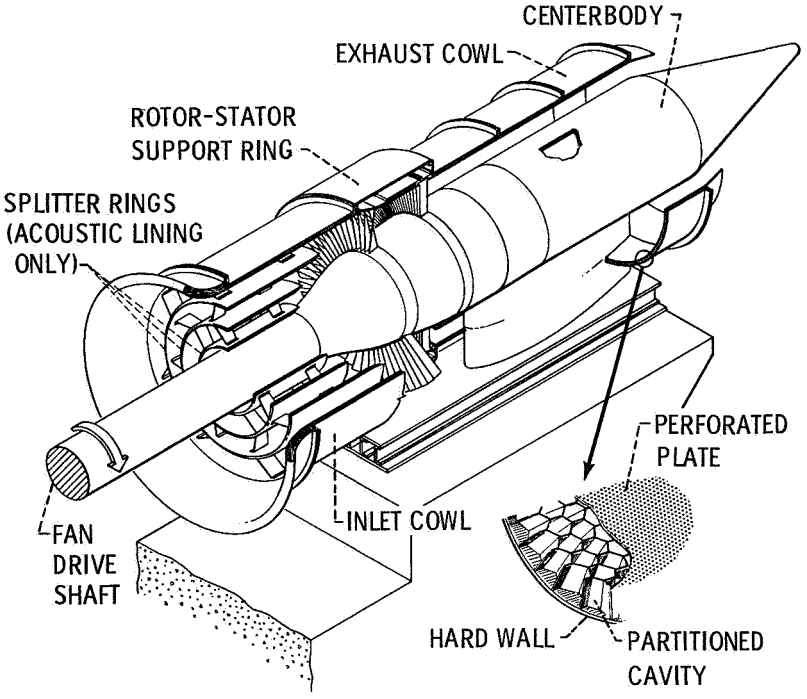

Figure 2. - Cutaway view of fan and suppressor assembly.

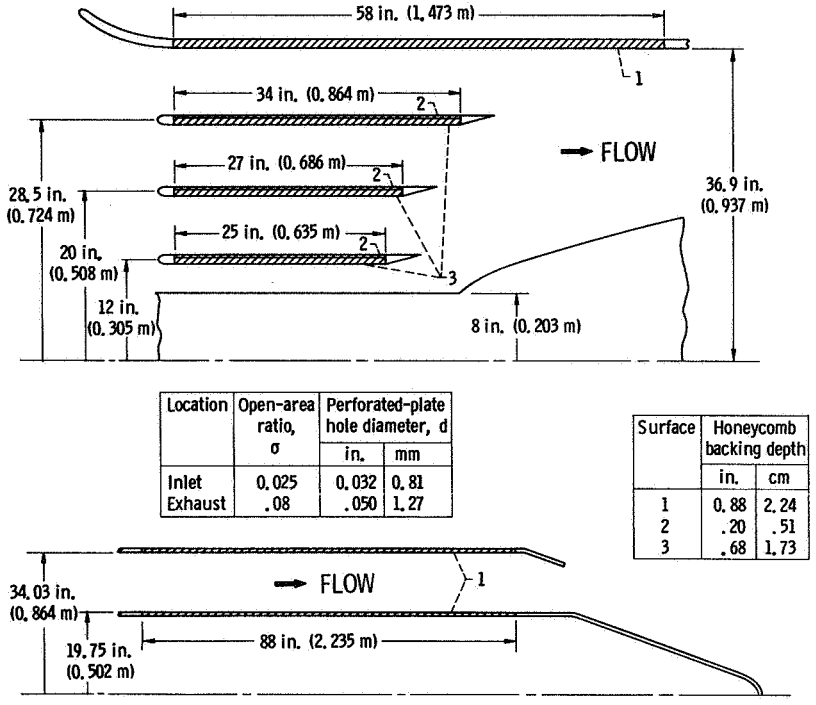

Figure 3. - Suppressor dimensions and materials. All perforated-plate sheet, 0.02-inch-(0.51-mm-) thick aluminum; all honeycomb, 3/8 inch (0.95 cm) hexagonal.

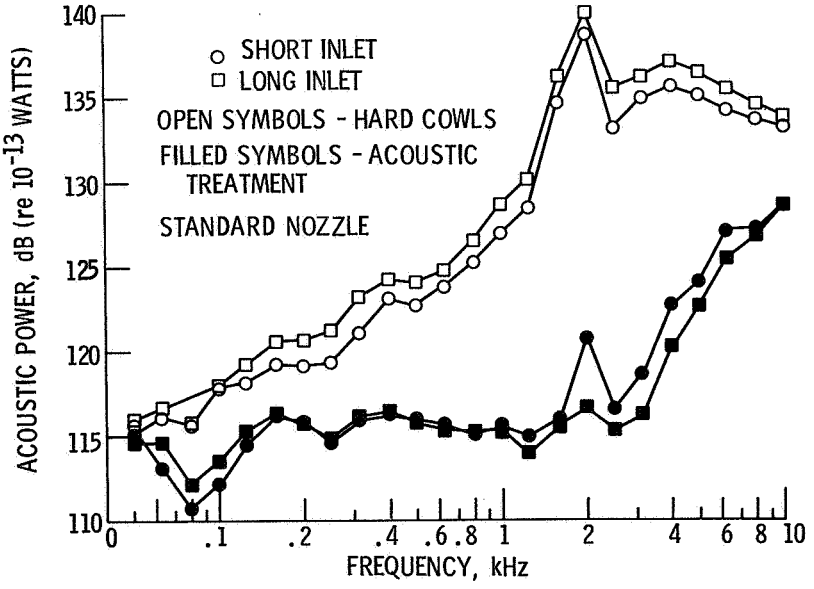

Figure 4. - Acoustic power spectra, front hemisphere, 60 percent speed.

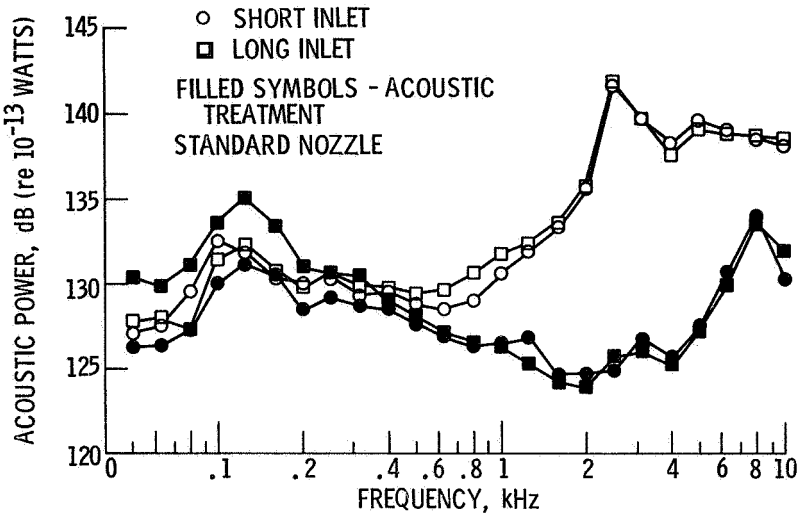

Figure 5. - Acoustic power spectra, rear hemisphere, 90 percent speed.

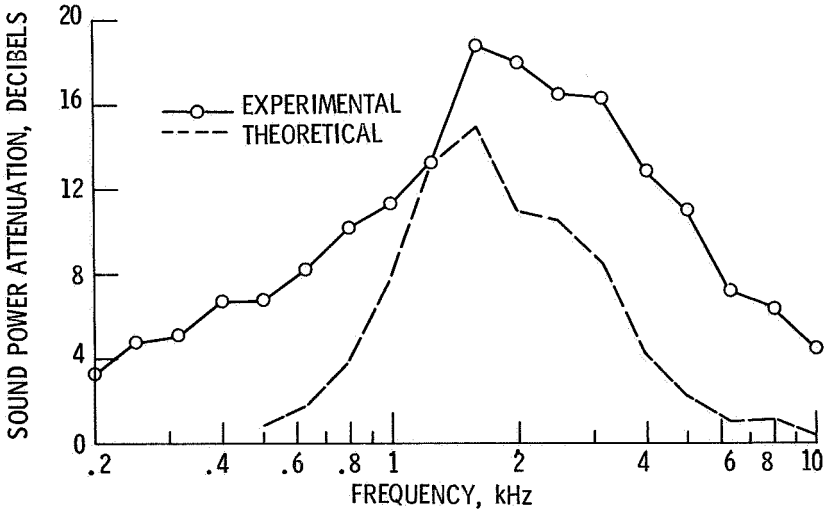

Figure 6. - Comparison of theoretical and experiment sound power attenuation, inlet, 60 percent speed.

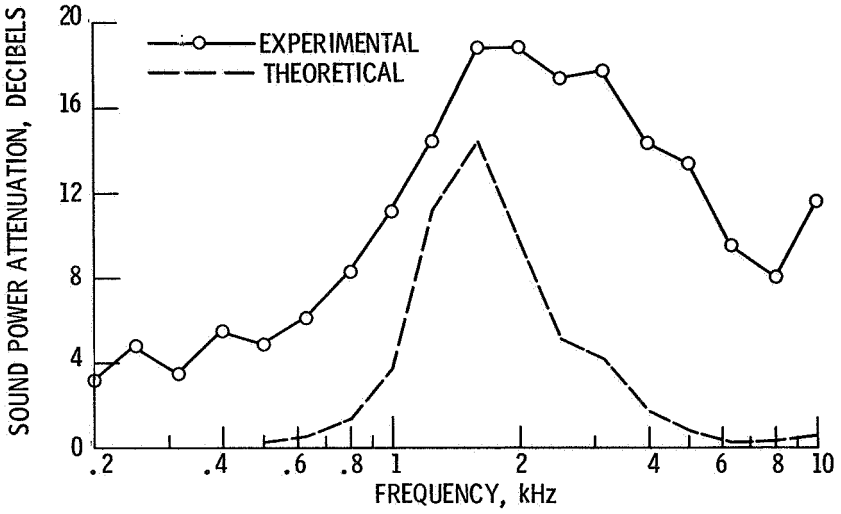

Figure 7. - Comparison of theoretical and experimental sound power attenuation, exhaust duct, 60 percent speed.

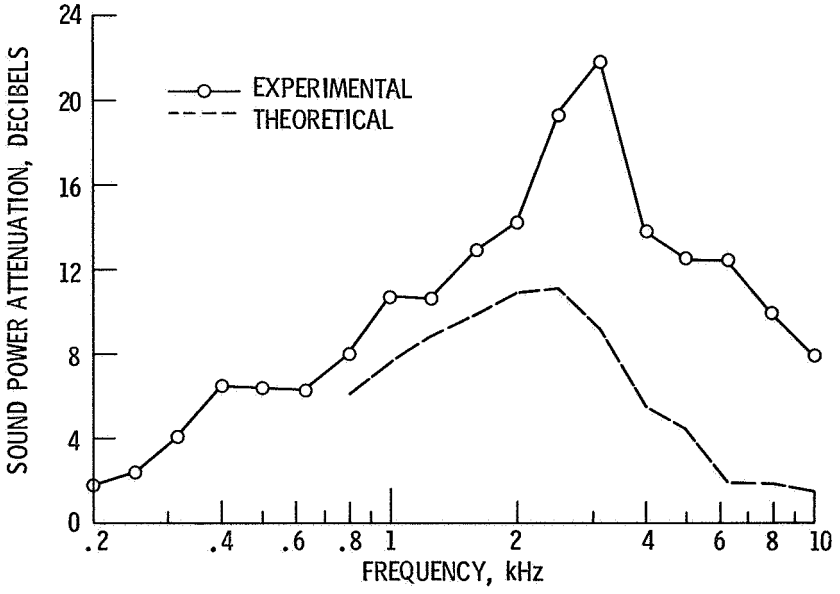

Figure 8. - Comparison of theoretical and experimental sound power attenuation, inlet, 90 percent speed.

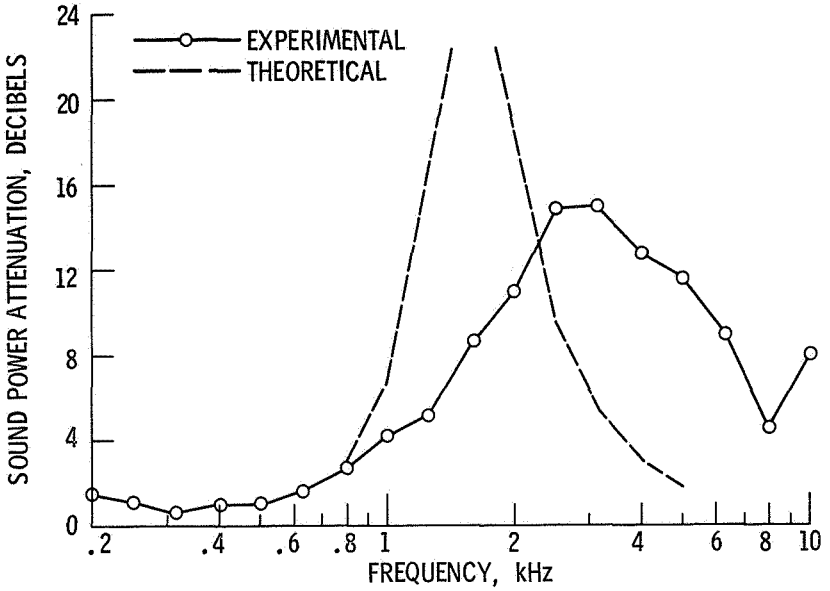

Figure 9. - Comparison of theoretical and experimental sound power attenuation, exhaust, 90 percent speed.

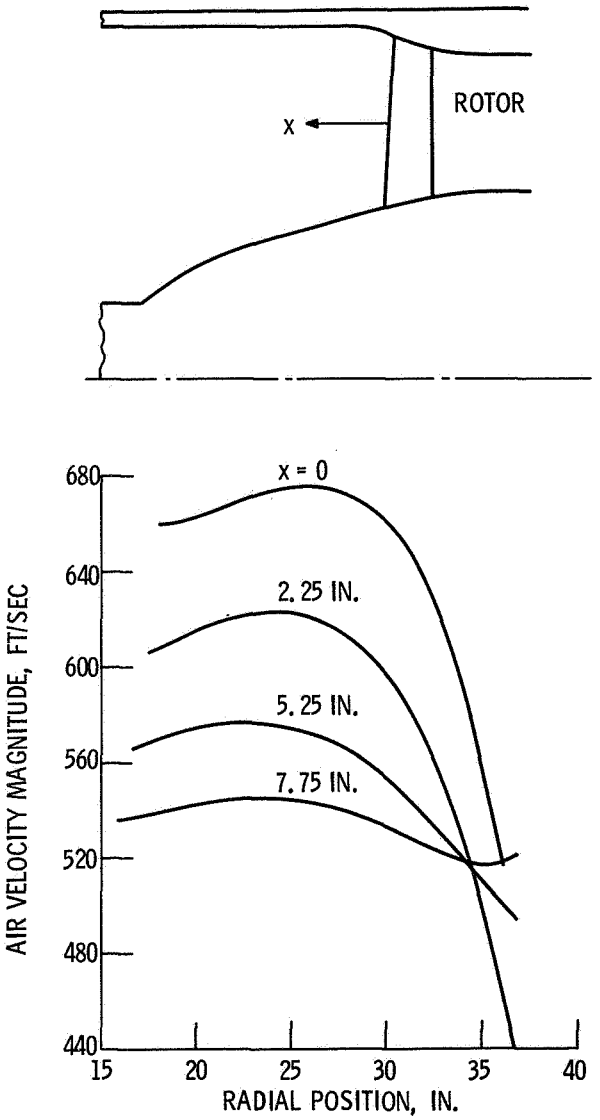

Figure 10. - Velocity profiles in the inlet, design speed.